Palaeogeography, Palaeoclimatology, Palaeoecology 517 (2019) 16–29

Contents lists available at ScienceDirect

Palaeogeography, Palaeoclimatology, Palaeoecology

journal homepage: www.elsevier.com/locate/palaeo

# The Silurian climatic transition recorded in the epicontinental Baltica Sea

Gambacorta G.*, Menichetti E., Trincianti E., Torricelli S.

*Eni S.p.A. Upstream and Technical Services, 20097 San Donato Milanese, MI, Italy*

ARTICLE INFO

*Keywords:*
Anoxia
Black shale
Epereic sea
Major and trace element geochemistry
Organic matter
Paleozoic

ABSTRACT

The transition from the Middle to Late Ordovician cold climate to the Silurian greenhouse phase was marked by major climatic and oceanographic changes. The vast epereic sea that during the early Paleozoic extended over the Baltic Plate for hundreds of kilometres recorded the dynamic processes that characterized this important climatic evolution. This shallow epicontinental sea experienced phases of hypoxic conditions for millions of years during the Silurian favouring the sedimentation of organic-rich deposits. A continuous core drilled in the Silurian fine-grained succession of the Baltic Basin was studied integrating sedimentological, palynological and geochemical data. The succession, deposited in a restricted environment in low-energy settings, recorded three long-term variations in bottom-water redox conditions. Our data highlight a direct control of long-term climatic changes on oceanic redox cycles. Phases of cool and dry climate with reduced runoff alternated with periods of warmer and humid conditions with higher runoff and fluvial discharge. During warmer and more humid climatic phases, the presence of a stable pycnocline hampered deep-water renewal efficiency, and together with increased nutrients led by enhanced weathering and runoff favoured the onset of anoxic bottom-water conditions. Cooler and drier intervals favoured instead a weaker and less stable pycnocline that, coupled with more oligotrophic conditions, drove the formation of oxic bottom-waters. The variation through time in water salinity and temperature influenced both the type of organic matter in the surface waters as well as its preservation along the water column. In fact, the extended residence time at the stable pycnocline during the anoxic phases led to the degradation of the organic matter and limited its accumulation at the sediment-water interface. The waning of the latest Ordovician cooling to the Silurian greenhouse climate was characterized by the progressive alternation of cool phases and warmer periods. The effect of this dynamic climatic instability on the redox state of the Baltica epicontinental sea protracted over millions of years up to the middle Silurian.

## 1. Introduction

The Silurian Period was characterized by important climatic and oceanographic changes. Following the early Paleozoic cooling (Late Ordovician–Early Silurian) (Page et al., 2007), Earth experienced a progressive warming and global sea-level rise (Melchin et al., 2013). The transition from the Hirnantian (latest Ordovician) glaciation peak, to the greenhouse phase was characterized by glacial maxima separated by warmer intervals (Page et al., 2007; Liu et al., 2017). In fact, ice-sheets dynamically expanded and retreated during the early Paleozoic, with glacial pulses occurring during the early Aeronian and late Telychian (Page et al., 2007). The termination of the glaciation was marked by widespread occurrences of oceanic anoxia occurring at all paleolatitudes (Cramer and Saltzman, 2007; Page et al., 2007; Le Heron et al., 2009; Melchin et al., 2013; Pohl et al., 2017). However, major uncertainties exist in the comprehension of the processes that controlled oceanic oxic-anoxic cycles and their relationship with global climate change during the Silurian.

Silurian ocean-bottom sediments preserved in the geologic record are scarce, thus hampering the overall understanding of the physical and chemical mechanisms that drove the variations in early Paleozoic oceans redox state (Melchin et al., 2013). However, the successions deposited on the vast epicontinental seas during this time interval represent a fundamental record of the early Paleozoic anoxic dynamics and their long-term evolution through time. A large shallow water sea extended for hundreds of kilometres over the Baltica plate during the early Paleozoic, whose sediments are now partially preserved in the lower Paleozoic shale belt in Poland (Jaworowski, 2000).

In the following, we present a detailed sedimentological, biostratigraphical and geochemical study of a continuous core drilled in the fine-grained Silurian record in the Baltic Basin in Poland. Our data yield intriguing insights into the climatically-driven changes in the ocean redox state during the early Paleozoic, at a time of major climate change from the Middle to Late Ordovician cold climate to the Silurian greenhouse conditions.

* Corresponding author.
*E-mail address:* gabriele.gambacorta@eni.com (G. Gambacorta).

https://doi.org/10.1016/j.palaeo.2018.12.016
Received 13 September 2018; Received in revised form 19 December 2018; Accepted 19 December 2018
Available online 27 December 2018
0031-0182/ © 2018 Elsevier B.V. All rights reserved.

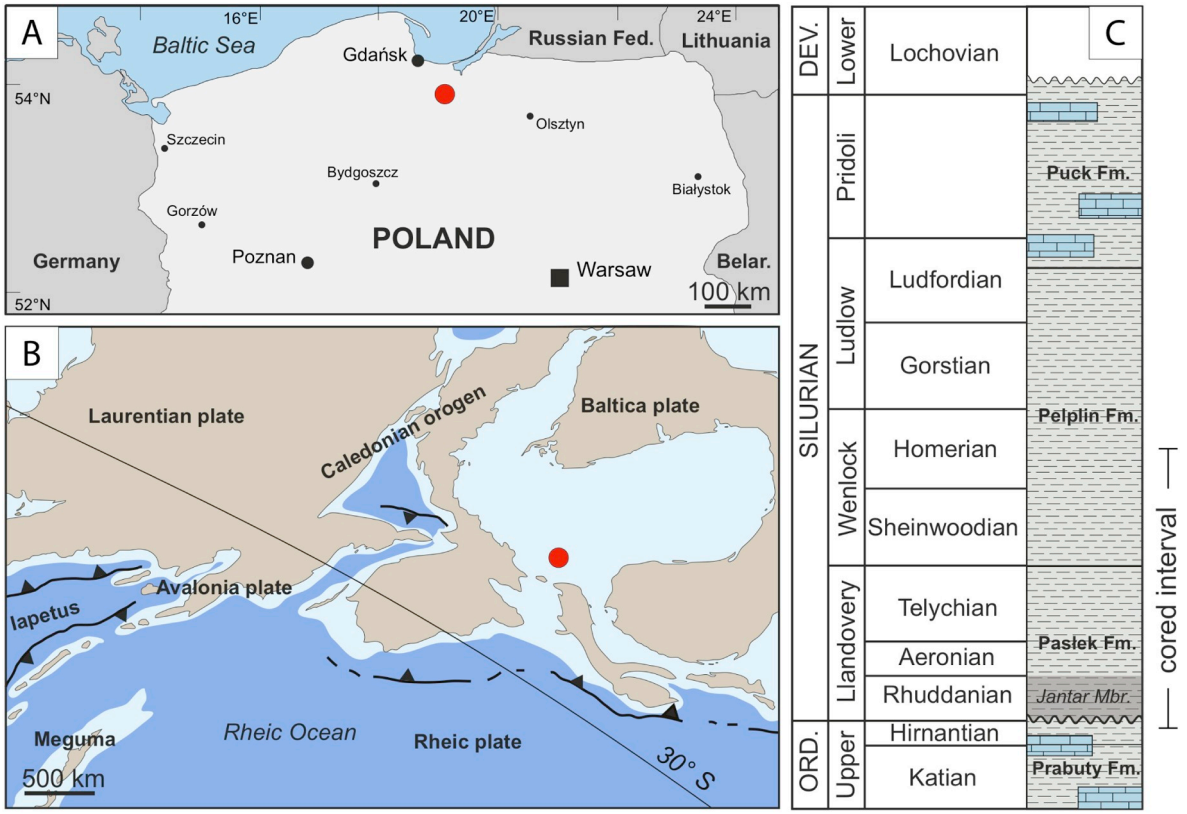


**Fig. 1.** A. Present-day geographic map. The location of the studied well is indicated by a red circle. B. Silurian (~425 Ma) paleogeographic map (modified after https://deeptimemaps.com/europe-series/). The paleogeographic position of the studied area is indicated by a red circle. C. Schematic stratigraphic chart of the Silurian in the Polish part of the Baltic region (modified after Modliński and Podhalańska (2010)). (For interpretation of the references to colour in this figure legend, the reader is referred to the web version of this article.)

## 2. Geological setting

The Silurian shale succession in Poland extends along the western margin of the East European Craton forming an almost 700 km-long undeformed belt oriented northwest (NW)-southeast (SE) that extends across the Baltic, Podlasie and Lublin basins (Porębski et al., 2013) (Fig. 1A). The Silurian shale succession deposited over a large shallow epicontinental ramp passing distally to the Caledonian foredeep (Porębski et al., 2013) with a limited communication with the Rheic Ocean (Fig. 1B). Sedimentation was accompanied by a low coarse detrital input with as major inputs the dispersal of calcareous detritus from the craton in the northeast and the input of silty sediments sourced from the Caledonian collision zone in the southwest (Jaworowski, 2000; Modliński and Podhalańska, 2010; Porębski et al., 2013).

The base of the Silurian succession is marked by a regional unconformity, Hirnantian to early Llandovery in age, that passes westward into a correlative conformity (Modliński et al., 2006; Modliński and Podhalańska, 2010). This erosive surface, that separates the marls and shaly marls of the Upper Ordovician Prabuty Formation from the Llandovery shales of the Pasłek Formation (Jaworowski, 2000) (Fig. 1C), is interpreted as the result of the forced regression related with the Hirnantian glaciations in Gondwana (Modliński et al., 2006; Modliński and Podhalańska, 2010). Early Silurian global warming induced a rapid post-glacial sea-level rise that accompanied the transgressive deposition of the first Silurian shales (Modliński et al., 2006; Modliński and Podhalańska, 2010). The Pasłek Formation (Fig. 1C) is characterized at the lowermost part by the black bituminous shales of the Jantar Member (Modliński et al., 2006). It passes then upwards into dark-grey and grey shales interlaminated with green, grey-green and black shales (Modliński and Podhalańska, 2010). The upper boundary of the Pasłek Formation is approximately early Wenlock in age (Modliński and Podhalańska, 2010) and marks the transitional passage to the grey to grey-green shales, rarely black shales, of the Wenlock-upper Ludlow Pelplin Formation (Modliński et al., 2006) (Fig. 1C). The Silurian succession then terminates with the upper Ludlow–Pridoli Puck Formation, characterized in the lower part by shales and calcareous laminated grey to green shales with rare bentonite layers, and in the upper part by laminated, grey-green calcareous shales, with interbeds and lenses of marly and organodetrital light grey limestones and marls (Modliński et al., 2006; Modliński and Podhalańska, 2010) (Fig. 1C).

## 3. Materials and methods

A 238-m-long continuous core drilled from a well located in the Baltic Basin in northern Poland (Fig. 1A) was described and analyzed for this study. This work integrates a mm-scale sedimentological description, mineralogical data, total organic carbon and Rock-Eval, palynofacies, and major and trace element geochemical data.

### 3.1. Sedimentological logging

Detailed bed-by-bed sedimentological description of the analyzed core was performed to capture any mm-scale variation in texture, composition and structures. Sedimentological description was also integrated with the total gamma-ray log (core gamma scan) directly measured on core by Schlumberger Reservoir Laboratories.

### 3.2. X-ray diffraction (XRD)

One hundred twelve samples were collected approximately every 2 m and analyzed for mineralogical characterization via X-ray powder

diffraction (XRD) using a PANalytical CubiX Pro instrument equipped with a CuKα (λ = 1.54178 Å) radiation source and a fast detector. The phase identification was made by a search-match procedure comparing the position and the relative intensity of the reflections with the data contained in a reference database. The quantitative bulk analysis was carried out by means of a full-profile fitting procedures based on the Rietveld method using SIROQUANT software.

### 3.3. TOC and Rock-Eval

Two hundred thirty samples were taken every metre and analyzed in order to measure total organic matter content (TOC) by means of LECO instrumentation. All the samples were also measured for source rock properties through Rock-Eval 6 analyzer. Thermal maturity was estimated with Tmax from Rock-Eval pyrolysis.

### 3.4. Palynofacies

The 112 XRD samples were also analyzed for palynofacies to characterize the organic matter type and monitor its variation through the succession. Samples were crushed and treated with 37% HCl and 38% HF, and sieved with 250 μm and 15 μm meshes. Heavy liquid separation with $ZnCl_2$ and centrifuging were performed to concentrate the residue. No oxidation was performed. Residue > 15 μm was mounted on two slides using Norland optical adhesive. Type and amount of organic particles were counted over nine vertical slide scans so distributed: 3 on the left side of the slide, 3 in the middle and 3 on right side of the slide, and finally converted to percentages.

### 3.5. X-ray fluorescence (XRF)

The above 112 samples were analyzed for major and trace element geochemistry using a PANalytical MagiX Pro WDXRF (wavelength dispersive X-ray fluorescence). Several calibration curves using standards were carried out in order to obtain quantitative elemental analysis for both major (i.e. Si, Ti, Al, Fe, Mg, Mn, Ca, Na, K, P) and trace elements (in abundances > 1 ppm; i.e. As, Ba, Co, Cr, Cs, Cu, Mo, Nb, Ni, Pb, Rb, Sc, Sr, Th, Tl, U, V, Y, Zn, Zr). In order to account for dilution effects elemental concentrations were normalized to Al. Concentrations are compared relative to the reference average crustal rocks or average shale (AS) element abundance of Wedepohl (1971, 1991) and expressed as element enrichment factors ($EF_{elem}$). Enrichment factors were computed using the following formula:

$$EF_{elem} = (element/Al)_{samp}/(element/Al)_{AS} \quad (1)$$

where $(element/Al)_{samp}$ is the ratio between the element and aluminum content in a sample, and $(element/Al)_{AS}$ is the ratio between the element and aluminum abundance in the average shale. We use hereinafter the term “enrichment” in samples with an $EF_{elem} \geq 5$, and on the contrary “depleted” when $EF_{elem} \leq 0.5$.

## 4. Results

### 4.1. Core sedimentological log

The lowermost part of the studied core recovered about 18 m of the Prabuty Formation (Fig. 2). The recovered unit is composed of grey-to-dark grey and rarely black marls with pyrite nodules. We observed highly erosive/condensed horizons and sporadic mm-to-cm-sized phosphate nodules. A well-sorted coarse sand bed with no internal structures is present at about 3214.5 m associated below and above with levels of limestone breccias. In the interval from 3206.0 to 3201.5 m we observed many volcanic ash beds yellowish to brownish in colour.

A series of erosional surfaces, with the major one at 3197.87 m, marks the lithological erosive contact between the Prabuty and the Pasłek Formation (Figs. 2 and 3A). In particular a sharp low gamma-ray value right at the contact between the two formations is observed, with values of < 50 °API in correspondence of an argillaceous limestone interval. The base of the Pasłek Formation is marked by a sharp rise in total gamma-ray from the average values of about 150 °API of the Prabuty Formation to about 250 °API (Modliński et al., 2006). The Pasłek Formation can be separated in two different intervals (Fig. 2). The lowermost one, from 3197.87 m up to about 3186.0 m is characterized by a grey-to-dark-grey slightly calcareous mudstone with frequent micro-conglomeratic beds with poorly-rounded limy to calcareous and shaly clasts (Fig. 3B) and calcareous marlstone beds with parallel to cross-laminations. Pyrite nodules are frequent (Fig. 3C) and bioturbations rare, in general *Chondrites* and *Planolites*. The upper interval is represented by rhythmic lithological alternations of greenish and dark grey-to-black shales (Fig. 3D). These varve-like mudstone couplets were interpreted as deposited under the orbital forcing on weathering intensity, nutrient supply and benthic anoxia (Gambacorta et al., 2018). Some beds present parallel laminations or wavy laminations and starved-ripples (Fig. 3E).

The contact with the above Pelplin Formation is transitional and is marked by the progressive disappearance of the greenish shale beds. It comprises grey-to-dark grey mudstones with frequent yellowish to brownish tephra layers (Fig. 3F). Mm- to cm-sized pyrite nodules are mainly present in the lowermost part of the formation (Fig. 3G). Calcite concretions in the form of nodules are common throughout the unit, with thicknesses on core spanning from about 5 to 35 cm (Fig. 3H). The deformation of the laminae within the mudrock surrounding the nodules suggests an early diagenetic origin of the concretions. In the uppermost part of the core we observed some limited bioclastic fragments, in particular at 2984.65 m where an almost cm-thick crinoidal bioclastic debris bed is present (Fig. 3I).

### 4.2. Mineralogical composition

From a mineralogical point of view the analyzed core is pretty homogeneous, remaining practically unvaried throughout the length of the core (Fig. 2). The sole exceptions are represented by the argillaceous limestone interval at the top of the Prabuty Formation and two samples at 3076 and 3050 m that show high amounts of calcite in correspondence of two nodular concretions. The carbonate fraction of the Silurian succession is on average about 6.9% of calcite, 5% of dolomite and 2.5% of ankerite. The siliciclastic part is mainly constituted by quartz in a fraction of about 35%, almost no K-feldspar (0.1% on average) and 7.4% of plagioclase. Total clay minerals plus micas represent on average about 37.8% of the total composition of the rock, with about 30.6% of illite “type” minerals, 1.6% of kaolinite and 5.7% of chlorite. Pyrite, with an average concentration of 4.8%, is present throughout the core with the exception of the interval between about 3180 and 3156 m where its concentration decreases to approximately 1.0%. Barite was detected with the XRD exclusively in 5 samples, around 3098–3096 m, 3076–3074 m and 2997 m.

### 4.3. TOC and Rock-Eval

Analyzed samples have in general a quite low average residual TOC content (Fig. 2). Higher TOC values were observed in correspondence of the lowermost part of the Pasłek Formation from the base of the unit up to about 3189 m with an average value of about 2.0 wt% and a peak up to 5.72%. The interval right above, from 3189 to 3165 m, shows a very low TOC content of about 0.25%. The interval 3165–3127 m is the second richest TOC interval with values of about 1.3%. TOC then decreases to values of about 1.1% up to 3090 m. Above this interval up to the top of the core TOC has values of about 0.8% on average, interrupted only by a small interval from 3042 to 3015 m with relatively higher TOC values of 1.1% on average with a peak up to 2.26%. Measured residual hydrogen index (HI) is quite low and stable

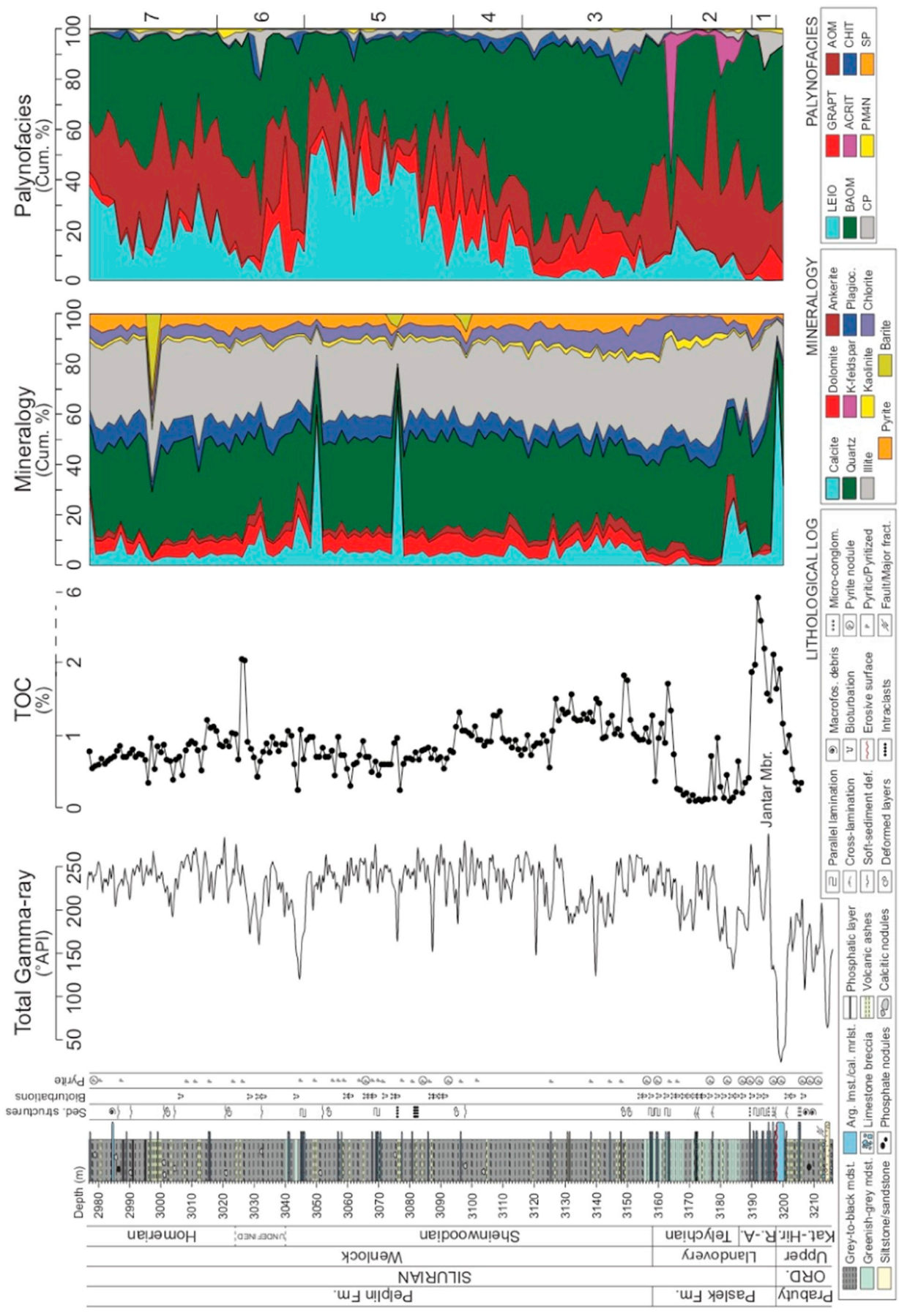


**Fig. 2.** Panel reporting from left to right: a schematic lithological column with sedimentary structures, bioturbations and pyrite occurrence; core total gamma-ray log; total organic carbon (TOC); mineralogical composition measured by means of XRD; the stratigraphic variation in palynofacies. See legends for lithological, mineralogy and palynofacies keys. Leiosphaeridia (LEIO); graptolite fragments (GRAPT); amorphous organic matter (AOM); black amorphous organic matter (BAOM); acritarchs (ACRIT); chitinozoans (CHIT); carbonized phytoclasts (CP); black needle-shaped palynomacerals (PM4N); spores and cryptospores (SP). Intervals 1 to 7 reported on the right side of the panel are defined and described in the text.

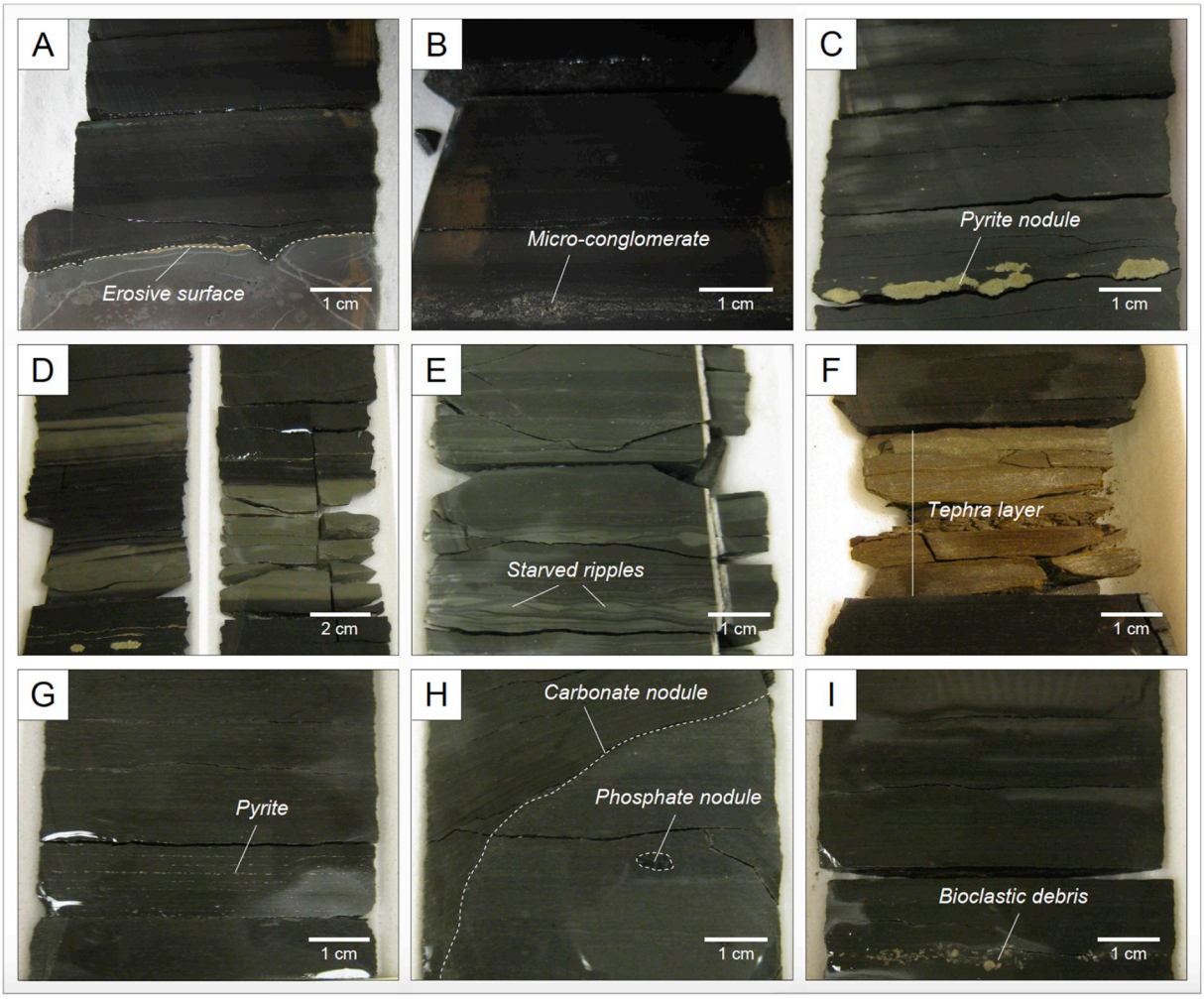


**Fig. 3.** Core photographs details of the slabbed core. A. Erosive surface marking the transition from the Ordovician Prabuty to the Silurian Pasłek Formation (3197.87 m). B. Micro-conglomeratic bed with poorly-rounded limy and shaly clasts (3196.8 m). C. Cm-scale pyrite nodules (3193.7 m). D. Rhythmic alternations of homogeneous greenish-grey mudstones and faintly laminated dark-grey-to-black mudstones (approximately 3177.5–3176.5 m). E. Starved ripples (3172.4 m). F. Tephra layer (3146.7 m). G. Mm-size pyrite micro-nodules lined along laminae (2987.75 m). H. Carbonate nodule (2985.3 m). I. Crinoidal bioclastic debris (2984.65 m).

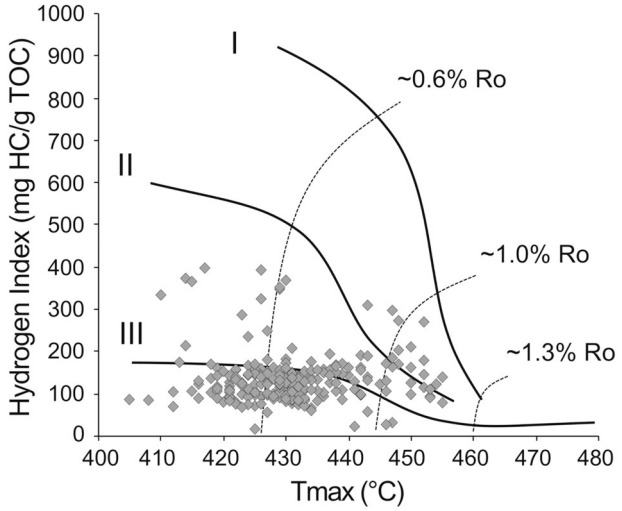


**Fig. 4.** Tmax versus HI diagram of all the measured samples. The maturity stages of analyzed samples are reported in terms of vitrinite reflectance (% Ro). Values lower than 0.6% indicate immature samples, mature (oil window) within 0.6–1.0% Ro, mature (gas window) in the range 1.0–1.3% Ro, while values higher than 1.3% Ro correspond to overmature samples.

throughout the core with an average value of 135 mg HC/g TOC. Tmax is on average 435 °C, with minimum values of 405 °C and maximum values of 455 °C, thus indicating maturity conditions spanning from immature to oil window. The Tmax versus hydrogen index plot reported in Fig. 4 highlights a dominant kerogen III type, which implies a prevailing contribution from terrestrially-derived organic matter.

### 4.4. Biostratigraphy and palynofacies

The biostratigraphy of the analyzed succession is mainly based on acritarchs occurrences. Chitinozoans are rare, discontinuous in the record and badly preserved, factors that prevented their use as reliable biostratigraphic markers. The studied core spans from the Upper Ordovician to the lower-middle Homerian (Upper Wenlock, Silurian) (Fig. 2). The Upper Ordovician (3216–3198 m) is identified on the basis of single occurrences of *Peteinosphaeridium* sp., *Peteinosphaeridium* cf. *velatum* and *Ordovicidium* sp. (Masiak et al., 2003; Delabroye et al., 2011). An almost non fossiliferous interval follows upwards from 3198 m to 3185.7 m and, based on its stratigraphic position, is interpreted as a Rhuddanian–Aeronian condensed section constrained at its top by the lowest occurrences of Telychian markers *Tylotopalla deerlijkianum* (Martin) Martin, 1978 and *Tylotopalla caelamenicutis* Loeblich, 1970. The highest occurrence of *T. deerlijkianum* at 3158 m and the

**Table 1**
Major and trace elements measured values. All oxides are reported as %, minor and trace elements in μg/g. All trace element/Al and Mn/Al ratios are expressed as $\times 10^{-4}$. Elements and element/Al standard deviation (1 σ) and maximum values are shown. Average shale (AS) values from Wedepohl (1971, 1991).

| Major and minor element concentrations and element/Al ratios in the studied core and average shale | | | | | | | | | |
|---|---|---|---|---|---|---|---|---|---|
| Element | Conc | Sigma | Max | Average shale | Element/Al | Conc | Sigma | Average shale | EF |
| $SiO_2$ | 53.3 | 6.0 | 69.6 | 58.9 | Si/Al | 3.39 | 0.52 | 3.11 | 1.1 |
| $TiO_2$ | 0.66 | 0.10 | 0.90 | 0.78 | Ti/Al | 0.053 | 0.003 | 0.053 | 1.0 |
| $Al_2O_3$ | 14.1 | 2.0 | 19.4 | 16.7 | – | – | – | – | 1.0 |
| $Fe_2O_3$ | 6.0 | 1.0 | 9.4 | 6.9 | Fe/Al | 0.56 | 0.06 | 0.55 | 1.0 |
| MgO | 3.7 | 0.5 | 4.9 | 2.6 | Mg/Al | 0.30 | 0.05 | 0.18 | 1.7 |
| CaO | 5.6 | 4.6 | 36.3 | 2.2 | Ca/Al | 0.65 | 1.10 | 0.18 | 3.6 |
| $Na_2O$ | 1.0 | 0.2 | 2.3 | 1.6 | Na/Al | 0.10 | 0.02 | 0.13 | 0.8 |
| $K_2O$ | 3.6 | 0.5 | 4.9 | 3.6 | K/Al | 0.40 | 0.02 | 0.34 | 1.2 |
| $P_2O_5$ | 0.08 | 0.01 | 0.13 | 0.16 | P/Al | 31.601 | 7.974 | 0.008 | 0.4 |
| As | 13 | 8 | 35 | 10 | As/Al | 1.7 | 1.1 | 1.1 | 1.5 |
| Ba | 1435 | 4034 | 27,017 | 580 | Ba/Al | 264 | 1036 | 66 | 4.0 |
| Co | 22 | 4 | 43 | 19 | Co/Al | 3.0 | 0.6 | 2.1 | 1.4 |
| Cr | 72 | 16 | 157 | 90 | Cr/Al | 10 | 2 | 10 | 1.0 |
| Cs | 3.3 | 2.1 | 8.5 | 5.5 | Cs/Al | 0.46 | 0.31 | 0.62 | 0.7 |
| Cu | 31 | 18 | 175 | 45 | Cu/Al | 4.3 | 2.3 | 5.1 | 0.8 |
| Mn | 683.36 | 858.67 | 7080.30 | 0.11 | Mn/Al | 114 | 255 | 96 | 1.2 |
| Mo | 9 | 4 | 17 | 850 | Mo/Al | 1.25 | 0.54 | 0.15 | 8.5 |
| Ni | 57 | 14 | 148 | 68 | Ni/Al | 7.82 | 1.99 | 7.7 | 1.0 |
| Nb | 13 | 2 | 16 | 18 | Nb/Al | 2 | 0.1 | 2 | 0.9 |
| Pb | 10 | 63 | 639 | 22 | Pb/Al | 1.3 | 8.4 | 2.5 | 0.5 |
| Rb | 124 | 17 | 163 | 140 | Rb/Al | 17 | 1 | 16 | 1.1 |
| Sc | 12 | 2 | 17 | 13 | Sc/Al | 1.6 | 0.3 | 1.5 | 1.1 |
| Sr | 143 | 99 | 1062 | 300 | Sr/Al | 21 | 22 | 34 | 0.6 |
| Th | 10 | 5 | 58 | 12 | Th/Al | 1.355 | 0.944 | 1.358 | 1.0 |
| Tl | 24.20 | 3.19 | 28.40 | 0.68 | Tl/Al | 3.308 | 0.656 | 0.077 | 43.0 |
| U | 5.7 | 1.9 | 14.4 | 3.7 | U/Al | 0.77 | 0.26 | 0.42 | 1.8 |
| V | 113 | 39 | 391 | 130 | V/Al | 15 | 5 | 15 | 1.0 |
| Y | 27 | 4 | 43 | 41 | Y/Al | 3.7 | 0.9 | 4.6 | 0.8 |
| Zn | 66 | 98 | 738 | 95 | Zn/Al | 10 | 18 | 11 | 0.9 |
| Zr | 162 | 23 | 234 | 160 | Zr/Al | 22 | 2 | 18 | 1.2 |
| TOC | 0.9 | 0.6 | 5.7 | 0.2 | – | – | – | – | – |

occurrence of *Salopidium granuliferum* (Downie) Dorning, 1981 at 3164 m indicate respectively the top and the upper part of Telychian (Jachowicz, 2000; Masiak et al., 2003; Molyneux et al., 2008). The absence of *T. deerlijkianum* from 3158 m upwards and the highest occurrence of *T. caelamenicutis* at 3040 m define the Sheinwoodian core section (Le Hérissé, 1989; Masiak et al., 2003). The Homerian interval is defined by the first appearance of *Evittia robustispinosa* (Downie) Lister 1970 at 3024 m (Le Hérissé, 1989).

The particulate organic matter present in the studied samples was grouped into nine categories hereinafter listed in order of quantitative importance (Fig. 2): black amorphous organic matter (BAOM), considered to represent degraded terrestrial plant debris (Whitaker et al., 1992); Leiosphaeridia (LEIO) (Tyson, 1995; Vecoli et al., 2009); amorphous organic matter (AOM), produced anaerobically in restricted and low-energy lacustrine and marine environments (shelf and deep offshore) (Tyson, 1995); graptolite fragments (GRAPT) (Egenhoff and Maletz, 2007), frequently observed at low paleolatitudes of the Baltica faunal province (e.g., Goldman et al., 2013); carbonized phytoclasts (CP), black, opaque, lath-shaped particles, derived possibly from oxidized or carbonized plant tissue of cryptospores-bearing plant vegetation (Whitaker et al., 1992; Tyson, 1995); PM4N (palynomaceral 4 needle-shaped, sensu Whitaker et al. (1992)), constituted by black needle-shaped fragments, opaque and structureless, considered buoyant and better preserved in low energy settings (Whitaker et al., 1992) (this palynomaceral is usually considered to originate from inertinitic material and in our record is very rare); chitinozoans (CHIT) (Vecoli et al., 2009); acritarchs (ACRIT) (Wicander and Wood, 1997); spores and cryptospores (SP) are the reproductive cells of bryophytes (mosses) and pteridophytic vascular plants (ferns).

Observed palynofacies show major fluctuations throughout the studied record (Fig. 2). The lowermost Interval 1 (3198–3190 m) is characterized by the dominance of BAOM and fair amount of AOM. Leiosphaeridia are very rare to absent and graptolite fragments show a relative peak. The structured fraction represented by CP, PM4N and SP components, exhibits here relatively high concentrations. The above Interval 2 (3190–3164 m) is still dominated by BAOM and AOM particles, whereas Leiosphaeridia increases and conversely graptolite fragments disappear. The structured fraction drops to lower values. Furthermore, two relative acmes of acritarchs are confined to this interval. A strong dominance of BAOM is evident within Interval 3 (3164–3118 m), whereas Leiosphaeridia decreases along with AOM. AOM records the lowest percentages from 3145.9 to 3122 m compensated by the reappearance of graptolite fragments. The structured components rise again to relatively high concentrations. Interval 4 (3118–3102 m) shows a transitional behavior in terms of palynofacies assemblages, with a progressive increase in Leiosphaeridia associated with the decrement of the BAOM and structured fractions. This trend continues in the following Interval 5 (3102–3046 m), with Leiosphaeridia becoming the dominant palynofacies component from 3082 to 3048 m. BAOM and structured components decrease to relatively low abundances. Interval 6 (3046–3018 m) records a sharp reduction of Leiosphaeridia matched by a limited increase of BAOM, and an acme of graptolite fragments in the lowermost part. The terrestrial structured components increase and AOM abundance increases back to its initial level (about 30%). The uppermost Interval 7 (3018–2977 m) shows a balanced palynofacies composition including Leiosphaeridia, BAOM and AOM, with Leiosphaeridia increased in number with respect to the interval below.

### 4.5. Major and trace element compositions

Average major and trace element concentrations, element/Al, standard deviation (1 σ) and maximum values of the analyzed samples in the Silurian interval are reported in Table 1. The average

composition of all the analyzed samples is quite similar to average shale (AS) values (Wedepohl, 1971, 1991) for most of the detected elements. In fact, average enrichment factor values are mostly around 1, thus in general giving no evidence of enrichment or depletion in comparison to AS, with the remarkable exception of Mo and Tl, with an enrichment factor on average of 8.5 and 43.0 respectively. Slightly enriched are also Ca (EF = 3.6) and Ba (EF = 4.0). Analyzed samples on average are only depleted with respect to P (EF = 0.4) and slightly to Pb (EF = 0.5) (Table 1).

## 5. Discussion

### 5.1. Depositional settings

The studied Silurian fine-grained sequence is characterized by very limited lithological variations as well as an almost constant mineralogical composition. With the exception of the calcareous concretions, the sediment is mainly composed by quartz and illite, with limited amounts of plagioclase, suggesting a predomination of the siliciclastic input over indigenous and/or allochthonous carbonate. > 80% of the clay minerals plus micas fraction is made of illite, thus not providing any indication of neither the proximity of the source based on clay mineral size distribution (Thyberg et al., 2000), nor changes from warm (kaolinite) to cool (chlorite) water conditions (Fagel, 2007). Samples elemental compositions are plotted on a triangular diagram with axes $Al_2O_3 \times 5$, $SiO_2$, and CaO in order to map the variation in the three major components of sedimentary rocks, i.e. clays, quartz and/or biogenic silica, and calcium carbonate respectively (Fig. 5). Almost all the samples fall in correspondence of AS composition, with very few of them lined on the so-called 'carbonate dilution line' connecting the AS point to the CaO pole. This graph is a further confirmation of a stable and homogenous background sedimentation with little contribution by carbonates ($EF_{Ca}$ = 3.6, Table 1). The almost constant concentrations of Ti, K and Rb (see low standard deviation values of Ti, K and Rb concentrations in Table 1), considered as lithogenic conservative elements (Koinig et al., 2003), indicate an essentially homogeneous detrital source area through time. Si, Ti and Zr concentrations, considered as proxies for detrital input (e.g. Schneider et al., 1997; Ganeshram et al., 1999; Sageman and Lyons, 2005), are quite similar to AS values (Wedepohl, 1971, 1991) (Table 1). This signal suggests a limited coarse-grained terrigenous detrital input in a distal depositional setting. The presence along all the studied interval of small *Planolites* and abundant *Chondrites* suggests that the deposition occurred under

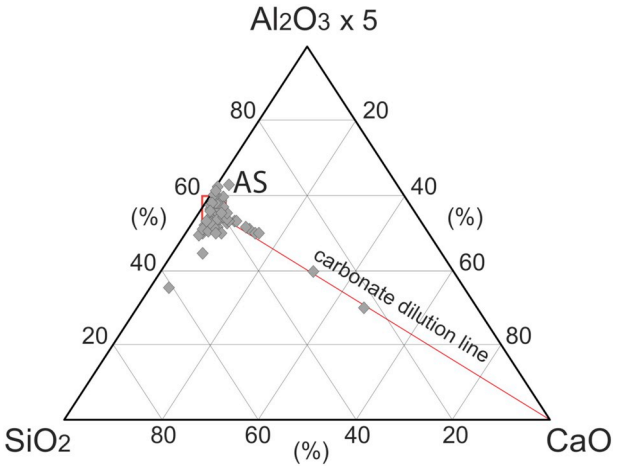


**Fig. 5.** Ternary diagram of relative proportions of $Al_2O_3$ (×5), $SiO_2$, and CaO. The average shale (AS) composition (Wedepohl, 1971, 1991) and the carbonate dilution line (red line) are reported. See text for details. (For interpretation of the references to colour in this figure legend, the reader is referred to the web version of this article.)

reduced-oxygen conditions (Bromley and Ekdale, 1984) from outer shelf up to bathyal water depths (Seilacher, 1967). Observed carbonate nodules represent instead an early diagenetic feature. We interpret the presence of the carbonate concretions as related to early dissolution of the calcium carbonate by aggressive interstitial waters. The reducing conditions and the preservation of organic matter probably favoured the formation of low-pH fluids undersaturated with respect to calcium carbonate capable of dissolving and redistributing the $CaCO_3$ in the form of concretions.

The high thallium enrichment ($EF_{Tl}$ = 43.0) needs a separate discussion. Many gases and particles are released during and between eruptions, such as carbon dioxide, water vapour, sulfur dioxide, hydrogen fluoride and hydrogen chloride together with important amounts of heavy metals such as Cd, Pb, Zn, Bi, Cr (Oppenheimer, 2011) and also Tl (Oppenheimer, 2011; Kellerhals et al., 2010). High Tl concentrations were also observed in volcanic active fumarole in the form of an orthorhombic of thallium iodide mineral called nataliyamalikite (Okrugin et al., 2017). Ash beds, as those we observed in the studied core, are frequently described in the Polish fine-grained Silurian sequence (Modliński and Podhalańska, 2010; Trela et al., 2017). However, the quite constant high Tl concentrations in all the analyzed samples (Table 1), not exclusively limited to those intervals with discrete ash beds, suggest that the ash material is likely dispersed within the fine-grained matrix throughout the studied succession. This pyroclastic material was probably sourced by the active subduction zone developed close to the southeastern side of Baltica and then transported in the atmosphere under the control of the SE trade winds (Trela et al., 2017).

### 5.2. Organic-matter variability

Measured kerogen III organic matter properties, as shown in the HI vs Tmax graph in Fig. 4, indicate a great contribution from terrestrially-derived organic matter. Observed palynofacies are in good agreement with what observed on Rock-Eval data. In fact, on average > 50% of the palynofacies is characterized by palynomaceral classes such as carbonized phytoclasts (CP), black needle-shaped phytoclasts (PM4N) plus great amounts of highly oxidized black amorphous organic matter (BAOM) of continental origin.

The composition and distribution of organic matter reflects the ecological conditions and the sedimentological processes of the depositional environment. Observed palynofacies indicate that the deposition occurred in low-energy marine conditions, as suggested by the AOM fraction ranging from 10% to 30% (Tyson, 1995), the occurrence of needle shaped fragments (PM4N) (Whitaker et al., 1992), and the common and regular presence of marine indicators such as Leiosphaeridia, acritarchs, chitinozoan and graptolite fragments. Some relative variations in sea level can be assessed on the basis of the observed palynofacies. The lowermost intervals 1 and 2 (Fig. 2) represent the shallowest depositional setting, as indicated by the scarcity of Leiosphaeridia and fair diversity of acritarch assemblages (Wicander and Wood, 1997). The appearance of chitinozoan and the flourish of graptolite fragments within intervals 3 and 4 suggest a water deepening (Egenhoff and Maletz, 2007). A relatively deep environment characterizes also intervals from 5 to 7.

Additional inferences can be done about the climatic conditions at the time of deposition. The Leiosphaeridia abundance in sediments of early Paleozoic is widely recognized as related to deposition under cold waters (Prauss and Riegel, 1989; Tyson, 1995; Warny et al., 2006; Moczydłowska, 2008; Vecoli et al., 2009), while Graptolites are associated with warm water conditions (Goldman et al., 2013). Leiosphaeridia and Graptolite fragments in our cored section show an inverse relationship (Fig. 2), not very sharp, but otherwise recognizable, that we interpret as possible fluctuations between periods of relatively cooler water conditions (Leiosphaeridia abundance/dominance) and periods of relatively warmer water conditions (Graptolite fragments

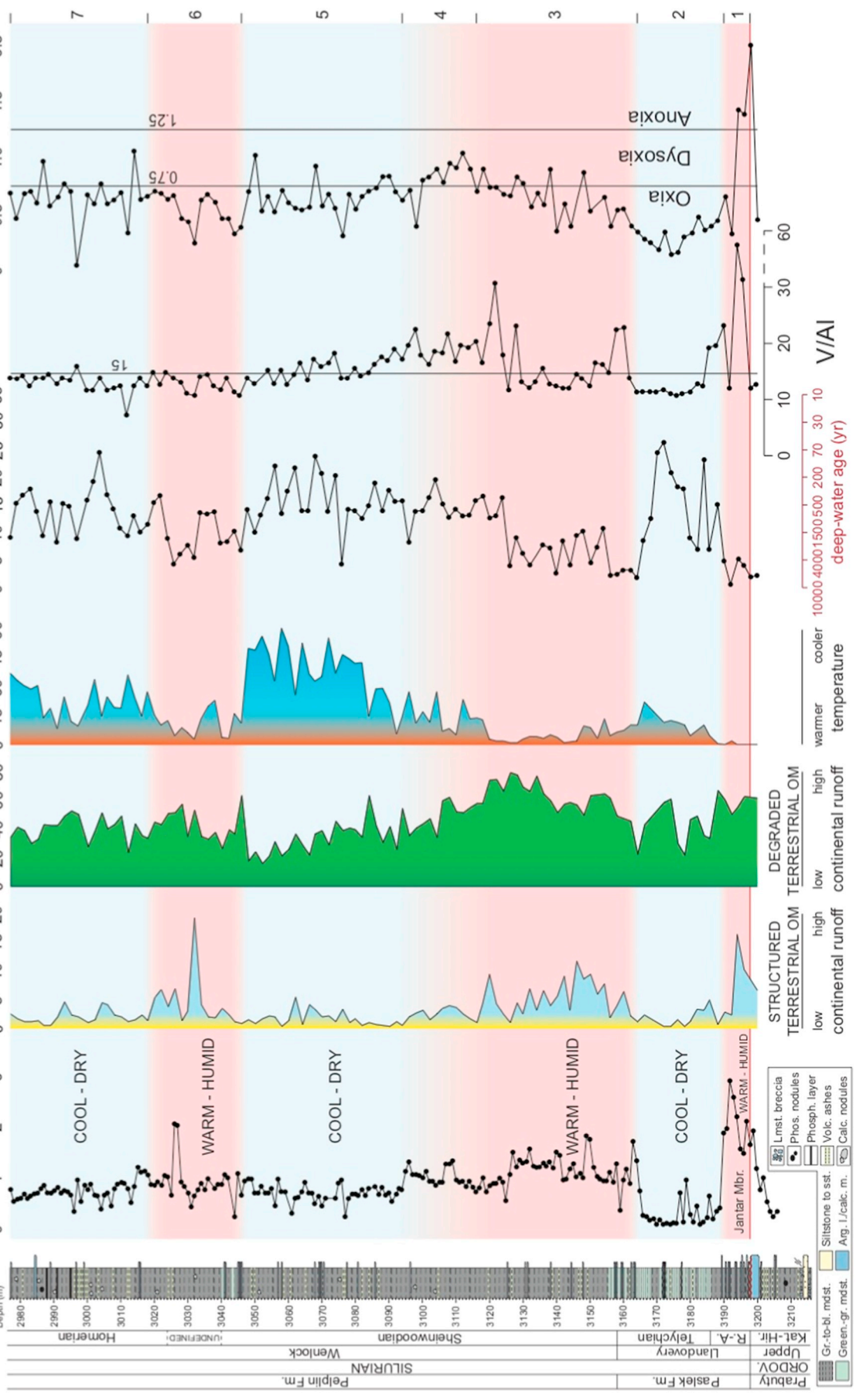


**Fig. 6.** Panel reporting from left to right: a schematic lithological column; total organic carbon (TOC); relative distribution of cumulative structured continental organic matter obtained as the summation of carbonized phytoclasts (CP), black needle-shaped phytoclasts (PM4N), spores (SP); continental black amorphous organic matter (BAOM); Leiosphaeridia (LEIO); redox sensitive (Mo/TOC, V/Al, U/Th) trace element stratigraphic distribution (values for deep-water age are estimated from Algeo and Lyons (2006)); schematic oxygen isotopic data ($\delta^{18}O_{phos}$) are from Trotter et al. (2016) (Anticosti Island, Canada – in green; Estonia and Latvia, Baltica – in light blue). The vertical line in the V/Al graph represents V/Al average shale (AS) composition according to Wedepohl (1971, 1991). U/Th redox thresholds are from Jones and Manning (1994). For the sake of readability of the continental organic matter graph, V/Al and U/Th axes are cropped. Background shading indicate the intervals interpreted as characterized by warmer and more humid climatic conditions, while the pale blue bars indicate the intervals associated with cooler and drier climatic conditions. See legends for lithological keys. Intervals 1 to 7 reported on the right side of the panel are defined and described in the text. (For interpretation of the references to colour in this figure legend, the reader is referred to the web version of this article.)

increase). Even though an additional effect of sediment dilution on Leiosphaeridia relative concentration cannot be excluded, we think that such variations cannot be exclusively explained in terms of dilution, but represent a climatic signal of cool water conditions. In the studied succession we observe a long-term cyclicity in the palynofacies associations. Throughout the studied record intervals dominated by the land-derived structured components (CP, PM4N and SP) and the highly degraded amorphous continental fraction (BAOM) alternate with Leiosphaeridia (LEIO) (Fig. 6). The continental fraction, represented by the CP, PM4N and SP, together with the BAOM came into the basin during periods of high runoff and fluvial input (Whitaker et al., 1992; McArthur et al., 2016), thus lowering marine surface water salinity, while Leiosphaeridia occurred during cool climate conditions (Prauss and Riegel, 1989; Tyson, 1995; Warny et al., 2006; Moczydłowska, 2008; Vecoli et al., 2009). The fluctuations of these two associations suggest that two different climatic and environmental regimes alternated during the studied interval. Phases of cool-dry periods with reduced runoff and normal surface water salinity, alternated with times of warmer and more humid conditions, leading to higher runoff and fluvial discharge into the basin (Fig. 6). The Rhuddanian succession (Interval 1) deposited during relatively warm conditions with high continental runoff. The transition to the Telychian record (Interval 2) is marked by a sharp decrease in the terrestrial fraction and the relative increase in Leiosphaeridia, that suggests a shift to relatively cooler conditions with reduced runoff and normal marine surface water salinity. The uppermost Telychian interval, at the transition from Interval 2 to Interval 3, indicates a sharp shift back to warm and humid conditions with high runoff and reduced surface water salinity that lasted at least for the lowermost part of the Sheinwoodian succession. The change to warmer settings is witnessed also by the presence of graptolites that dominate within Interval 3 over Leiosphaeridia (Goldman et al., 2013). The passage to the upper Sheinwoodian record (Interval 4) is marked by the progressive shift to the cooler and drier conditions that characterized the whole Interval 5. Leiosphaeridia show in fact their highest abundance within Interval 5 concurrently with the decline of BAOM. Leiosphaeridia may represent 50% of the palynofacies composition, thus suggesting the change from warm to cool climate. Another pulse of relatively warm and humid conditions with high runoff occurred in correspondence of Interval 6 at the transition from the Sheinwoodian to the Homerian. In fact, this interval records a dramatic drop of Leiosphaeridia matched by a new acme of graptolite fragments at the base of the interval, while the land-derived phytoclasts show another positive fluctuation. Finally, the uppermost part of the studied record (Interval 7) marks the re-establishment of a cool and dry climate with limited fresh water input. We speculate whether the relative higher abundance of BAOM in this interval compared to other cool-dry episodes could be associated to the migration of Baltica towards lower latitudes and therefore relatively more humid conditions (Torsvik and Cocks, 2016).

### 5.3. Paleoredox and paleohydrographic conditions

The stratigraphic variation of redox-sensitive elements indicates that redox conditions varied through time alternating oxic phases with others characterized by dysoxia to persistent anoxia. V/Al and U/Th were used as tracers of the variation in redox conditions along the analyzed succession (Algeo and Maynard, 2004; Tribovillard et al., 2006; Piper and Calvert, 2009). Jones and Manning (1994) proposed values of the U/Th ratio lower than 0.75 as characteristic of oxic water column conditions, values between 0.75 and 1.25 of dysoxic settings and a U/Th ratio values > 1.25 as indicative of an anoxic depositional environment. V/Al and U/Th ratios (Fig. 6) show truly anoxic conditions only in correspondence of the Rhuddanian–Aeronian interval, from 3197.87 to 3194 m. In correspondence of the Telychian interval, from 3194 to 3164 m, bottom-water conditions progressively shifted to prevailing oxic conditions. Hypoxic water settings were re-established from 3164 to about 3122 m, followed then by a progressive shift back to prevailing oxic conditions from 3086 m up to the top of the studied core.

Moreover, U-Mo covariation in marine sediments can give important information on watermass conditions at the time of deposition and help in discriminating restricted over open unrestricted marine settings (Algeo and Tribovillard, 2009; Tribovillard et al., 2012). In fact, modern oxygen-poor marine environments show three different U-Mo covariation patterns (Algeo and Tribovillard, 2009). In particular, unrestricted upwelling environments show a peculiar trend characterized first by a preferential uptake of $U_{auth}$ in suboxic conditions and then by a progressive enrichment in $Mo_{auth}$ in sulfidic conditions. The second trend, peculiar of basins characterized by weakly restricted conditions, shows strong enrichment of $Mo_{auth}$ with respect to $U_{auth}$ at all EFs. The process responsible of this chemical behavior seems to be the "particulate shuttle" linked to Mn-Fe redox cycling within the water column. Finally, a third different trend is observed in those basins characterized by stable restricted conditions. In fact, where strongly restricted conditions prevent an efficient deep-water renewal, basin watermass becomes progressively depleted in aqueous Mo, thus determining a decrease of the $(Mo/U)_{auth}$ ratios with increasing EFs. The U versus Mo enrichment factors plot of analyzed samples is reported in Fig. 7. The relative enrichment of Mo respect to U at all EFs of almost all the analyzed samples, indicates that "particulate shuttle" drove the accumulation of Mo versus U (Algeo and Tribovillard, 2009; Tribovillard et al., 2012). The observed trend indicates that the deposition of the studied succession occurred under strong variations in water column redox conditions at short to intermediate timescales (Algeo and Tribovillard, 2009). However we speculate whether "particulate shuttle" coupled with the "basin reservoir effect" (Algeo and Lyons, 2006) can be at the origin of the observed enrichment in Mo ($EF_{Mo}$ = 8.5) without an enrichment in all the other redox-sensitive elements (Table 1). As observed in the modern Orca Basin (Tribovillard et al., 2008 and references therein), restricted conditions prevent an efficient recharge of the watermass chemical reservoir, inducing the formation of deep-watermass depleted in redox-sensitive metals. Despite the trace metal drawdown in the watermass, particulate shuttle is capable of accumulating sediments enriched in Mo while poor to no enrichment in the other redox-sensitive elements occurs. As a consequence, although the composition in redox-sensitive elements and in particular the here used V/Al and U/Th ratios preserves the long-term hypoxic–oxic variations at time of deposition, it can potentially underestimate the real depositional paleoredox conditions of the studied

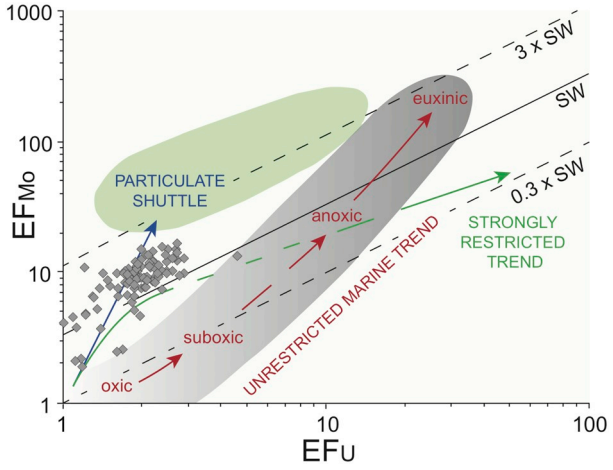


**Fig. 7.** Logarithmic plot of $EF_U$ versus $EF_{Mo}$ for the analyzed samples. The principal trends reported follow Algeo and Tribovillard (2009) and Tribovillard et al. (2012). Black lines show Mo/U molar ratios equal to the seawater value (1 × SW) and to fractions thereof (0.3 × SW, 0.1 × SW). See text for explanation.

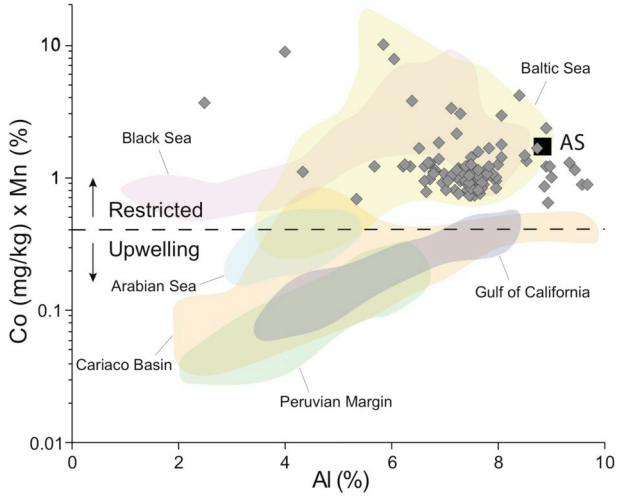


**Fig. 8.** Al vs Co × Mn graph. The distinction between upwelling (< 0.4) and restricted settings (> 0.4) follows the cut-off value of ~0.4 proposed by Sweere et al. (2016). The relative composition of modern anoxic basins is shown with different coloured shades following the data presented in Sweere et al. (2016). (For interpretation of the references to colour in this figure legend, the reader is referred to the web version of this article.)

succession.

Cobalt and Mn represent an additional proxy capable to discriminate between hydrographic restricted versus open marine upwelling settings, as proposed by Sweere et al. (2016). They mapped the different behavior with respect to these two elements of nine different present-day sites characterized either by hydrographically restricted conditions or continental margin upwelling settings. Sweere et al. (2016) noticed that in restricted basins Co and Mn concentrations are commonly near (or above) reported crustal abundances, while organic-rich sediments deposited in modern upwelling areas and the Cariaco Basin are generally depleted in Co and Mn. They identified a cut-off value in the Co × Mn index of about 0.4, that separates restricted settings with typically Co × Mn values > 0.4 and upwelling settings lower than 0.4. Cobalt × Mn composition of analyzed samples, reported in Fig. 8, show values ranging from about 0.6 up to about 10.0, with the vast majority of the samples distributed within a range of values of about 0.7–1.5. In particular our data, when compared with the Al vs Co × Mn composition of modern hydrographically restricted basins, show values comparable with the organic-rich sediments collected in the Baltic Sea in the Bornholm and Arkona basins and in TOC-rich deposits in the Black Sea (Sweere et al., 2016). This pattern indicates that bottom-water anoxia was likely connected with poor vertical mixing and deep-water ventilation restricted conditions.

All modern hydrographic restricted basins, although sharing poorly efficient deep-water circulation, differ considerably in terms of sill and chemocline depth and deep-water age (Algeo and Lyons, 2006 and references therein). The Mo/TOC ratio can give important information on basin paleohydrographic settings at the time of deposition (Algeo and Lyons, 2006). Under reducing conditions Mo flux in the water column is mainly associated with sedimentary organic matter sinking and burial. In restricted basins, where basin physiography does not allow an adequate resupply of Mo by deep-water renewal, basin watermass gets progressively depleted in Mo. Therefore, under poorly efficient circulation conditions, deposited organic matter becomes progressively more and more depleted in Mo which consequently increasingly lowers the Mo/TOC ratios (Algeo and Lyons, 2006; Rowe et al., 2008; Algeo and Rowe, 2012). Furthermore, an estimate of deep-water age renewal by means of the Mo/TOC ratio can be defined (Algeo and Lyons, 2006). The stratigraphic variation of the Mo/TOC ratio in the studied samples (Fig. 6) indicates that basinal paleohydrographic conditions varied through time. In particular, the lowermost Rhuddanian–Aeronian interval, characterized by the most extreme anoxic conditions, presents the lowest Mo/TOC values (about 2) of the whole studied Silurian succession. We can estimate for this interval a deep-water renewal time of about 6500 years. Together with the establishment of the oxic conditions observed in correspondence of the 3194–3164 m interval, the Mo/TOC ratio progressively rises to values up to about 25. These values suggest that the deposition of this interval occurred under more efficient circulation conditions, with a deep-water renewal age of about 100 years. With the re-establishment of the hypoxic conditions (3164–3122 m) the Mo/TOC ratio decreases back to an average value of 5, that indicates a deep-water renewal time of about 4500 years. From 3122 m upwards, with a transition sharper than that observed on the V/Al and U/Th ratios, the Mo/TOC proxy moves back to conditions of more efficient circulation with a deep-water age of about 400 years (Mo/TOC ~ 16). A third phase of stagnation with a deep-water renewal time of about 2000 years occurs in correspondence of the interval from 3046 to 3024 m, where we recognized a decrease of the Mo/TOC ratio back to values of about 8. Differently from what observed in the previously described units, this low Mo/TOC interval is not reflected on a variation towards hypoxic conditions. We interpret this unit as deposited under slightly restricted paleohydrographic conditions not sufficient to develop benthic hypoxia. Finally, above this interval the Mo/TOC ratio rises again back to values of about 16.

The dynamic watermass redox variations observed in our record suggest that estuarine circulation probably acted in combination with hydrographic restriction in determining watermass stratification, as described in modern areas like Black Sea and Baltic Sea (Algeo and Lyons, 2006; Algeo et al., 2008; Algeo and Heckel, 2008). However, the assumption of a "superestuarine circulation model" (Algeo and Heckel, 2008), characterized by the sole inference of a shallow and laterally unbounded pycnocline, cannot be considered as the unique driver for watermass stratification in the analyzed record. In fact, such mechanism would determine a different behavior in the redox proxies, such as those observed for example in the Late Pennsylvanian Midcontinent Sea (Algeo and Heckel, 2008; Algeo and Tribovillard, 2009). There, the trend of $EF_{Mo}$ versus $EF_{U}$ shows variable but commonly high EFs, with covariation trend lines nearly parallel to the seawater molar ratio lines, and $(Mo/U)_{auth}$ ratios that are mostly between 0.1 and 1 times that of seawater. Moreover, the fact that our data show an Al vs Co × Mn composition comparable with the organic-rich sediments deposited in the modern Baltic Sea and Black Sea can be considered a further evidence of the contribution of hydrographic restriction and strong estuarine circulation to widespread anoxia. However in the future, the assessment of the amount of variability in redox conditions across the region could improve the comprehension of the relative importance of the two processes and their inference on the pycnocline.

### 5.4. Paleoceanographic and paleoclimatic implications

Two different climatically-driven depositional styles alternated during the sedimentation of the studied succession. During humid and warmer climatic conditions (Fig. 9A), intense runoff lowered basin surface water salinity and led into the basin large amounts of continental organic matter, while the generally warmer settings increased sea-surface temperature. The resulting water salinity and temperature stratification favoured the onset of a strong and stable pycnocline that established a poorly efficient bottom-water circulation, as reflected by the decrease in the Mo/TOC flux ratios. Moreover, the increased temperatures and humidity favoured intense weathering and runoff. As a consequence, large amounts of nutrients were delivered into the basin thus enhancing primary productivity. This process contributed to the establishment of water column anoxia (Pohl et al., 2017). The reduced exchange with oxygenated waters from the open ocean coupled with the estuarine water circulation and the oxidation of the organic matter resulted in the de-oxygenation of basin deep-water masses. We suppose

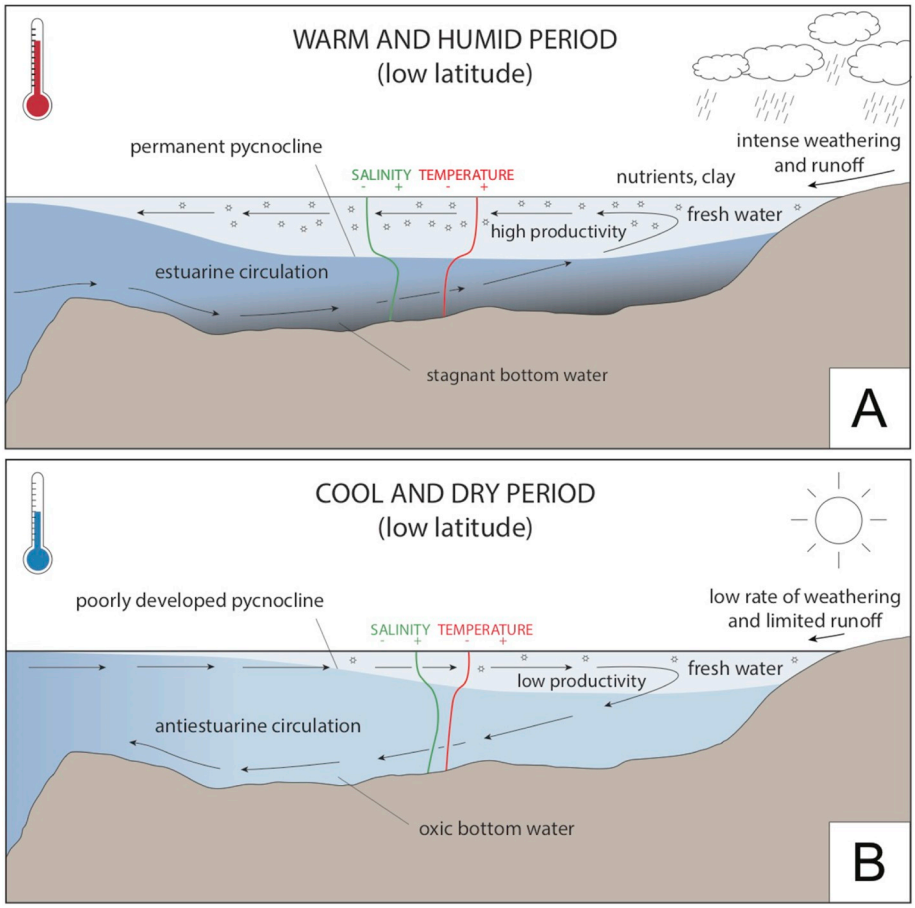


**Fig. 9.** Schematic depositional model (not to scale) representing the Silurian long-term anoxia dynamics in the epicontinental Baltica Sea during anoxic (above) and oxic (below) phases. See text for details.

that the presence of a stable pycnocline was capable of trapping organic matter for a sufficiently long time to allow its extensive degradation, thus resulting in the observed low TOC and HI organic matter properties measured in the studied record. A similar process was proposed by Tribovillard et al. (2008) to explain the TOC content generally lower than 1% and HI values on average between 100 and 200 mg HC/g TOC of the modern sediments deposited in the Orca Basin. Completely different hydrodynamic settings characterized the arid and cooler climatic phases (Fig. 9B). During these intervals the decrease in fresh water input increased sea-surface salinity and the cool water conditions favoured the bloom of Leiosphaeridia algae. Consequently, the salinity and temperature contrast existing between shallow- and deep-water masses reduced. In addition, the hampering of weathering and runoff limited the delivery of nutrients into the basin. The resulting progressive weakening of both pycnocline and the establishment of more oligotrophic conditions favoured deep-water circulation and stable benthic oxic conditions.

These two different patterns alternated with variable intensity throughout the studied Silurian record (Fig. 6). The lowermost part of the core, in correspondence of the early Silurian global warming and rapid post-glacial transgression (Modliński et al., 2006; Modliński and Podhalańska, 2010), records the highest anoxic conditions of the whole analyzed sedimentary succession. The coupling of the relatively rapid flooding of vast shallow areas of Baltica, poorly connected with the Rheic ocean, and the warm and humid conditions were probably at the origin of the onset of the observed hydrographic restriction. In particular, anoxia was particularly intense during the early transgressive phase, right above the Ordovician/Silurian unconformity. We speculate that, during the early phases of sea level-rise, the low sill depth was responsible of the peak in restriction experienced at the base of the transgression. Moreover, the release of nutrients during the weathering and the leaching of newly-exposed glaciogenic sediments might have further contributed to the establishment of the observed anoxic conditions (Pohl et al., 2017). The cooler and drier climate that characterized the Telychian progressively changed bottom-waters from anoxic to prevailing oxic conditions. With the uppermost Telychian a second phase of warm and humid climate gave rise to a second peak of hypoxic bottom-waters that persisted up to the lower Sheinwoodian. In the mid-upper Sheinwoodian climate then gradually changed to oxic cooler and drier conditions. At the transition between the Sheinwoodian and the Homerian a third phase of higher temperatures and humidity induced again a restricted paleohydrographic regime. The overall trend, on the basis of the palynological data and paleoredox (V/Al and U/Th ratios) and paleohydrographic (Mo/TOC) proxies, suggests a progressive waning through time in the degree of basin restriction. In fact, water column stratification and deep-water anoxia became less and less intense from the older to the younger hypoxic phases. The mechanisms that led to the termination of the early Paleozoic cold climatic phase are still under debate. Nonetheless, the cyclical alternation of two stable climatic modes could represent the peculiar response to the transition from cold to greenhouse global conditions during this time interval. The deposition of organic-rich sediments would then constitute a fundamental driver of this climatic change. We speculate whether the lower and lower availability of newly-exposed glaciogenic sediments might have had an impact on the total amount of available nutrients and their delivery into the oceans (Pohl et al., 2017). Such process would have concurred in hindering the onset of hypoxia trough time. Moreover, the observed coupling of warm and humid

conditions didn't necessarily extend after the climatic transition to the stable greenhouse conditions. This would have resulted in a warmer climate not substained by intense runoff and nutrient delivery. On a local scale, the observed progressive relative sea-level rise might have also contributed to a more efficient deep-water circulation. In fact, a higher sea-level would have reduced the impact of possible sills. The additional effect of the tectonical evolution of the basin physiography could have also contributed. We cannot exclude that crustal deformation, associated with phases of enhanced tectonics, could have resulted in a more efficient connection with the open ocean. However, the progressive docking of Baltica and Laurentia would have more likely led to a progressively more restricted basin physiography and to a consequent shift to more hypoxic conditions through time. As we do not observe such trend in our data, we think that tectonic activity cannot be considered as the only driving mechanism that led towards prevailing oxic conditions and a more efficient deep-water circulation through time.

### 5.5. Climatic cycles during the Silurian transition from glacial to greenhouse conditions

The traditional view of the Silurian as an environmentally stable period in Earth history, characterized by greenhouse conditions with a moderate latitudinal climate gradient (Calner, 2008), has been progressively undermined by the geological literature of the last decades. In fact, available data suggest that the Silurian was instead characterized by relevant oscillations between different climatic modes, associated with prominent cyclical lithological and faunal changes (Jeppsson, 1990; Aldridge et al., 1993; Jeppsson et al., 1995; Jeppsson, 1996, 1997; Bickert et al., 1997; Cramer and Saltzman, 2005, 2007; Page et al., 2007; Calner, 2008; Trotter et al., 2016, Liu et al., 2017). The seminal work of Jeppsson (1990) posed the first basis for the Silurian climatic shifts. He identified two discrete stable oceanic-climatic states that he named 'Primo and Secundo episodes' that alternated cyclically during the Silurian as a function of the cyclical shift of deep-water formation from high to low latitudes. In particular, according to his model, Primo episodes (P) were characterized by cold high latitudes and humid low latitudes, with well-oxygenated deep-waters and the deposition of organic-rich clay on shelves. Secundo episodes (S) were instead associated to relatively warm high latitudes and arid low latitudes, with inefficient circulation and formation of anoxic bottom waters in the oceans and the concurrent expansion of carbonate deposition on shelves. Bickert et al. (1997) partially revised this model on the basis of stable oxygen isotopes in brachiopods shells from the Silurian of Gotland (Sweden). They excluded the temperature control on the observed cyclicity by ascribing the variation in $\delta^{18}O$ to variations in salinity rather than to changes in temperature. For this reason, their model distinguishes arid periods (A-periods) from humid periods (H-periods) controlled by cyclical global changes in the evaporation-precipitation rates and rate of continental run-off. Cramer and Saltzman (2005, 2007) expanded the Jeppsson's (1990) model focusing on the meaning of the early Sheinwoodian Ireviken carbon isotope record. Following their model, the observed $\delta^{13}C$ positive excursion was the result of enhanced burial of organic carbon in deep waters during the Secundo episodes. Furthermore, Cramer and Saltzman (2007), focusing on the relative sea-level control on black shales occurrence, proposed that Primo state were favoured during transgressions due to increased primary productivity, while Secundo state would be associated with highstand due to the failure of the downwelling at higher latitudes and the waning of the thermohaline circulation. Page et al. (2007) went beyond the dichotomy between shelves and deep oceans by focusing on the general occurrence of black shales. They stated that oxic versus anoxic conditions were controlled by glacioeustatic sea-level variations, with black shales deposition occurring during deglacial transgressions, and well oxygenated deep-waters conversely occurring during the regressive phases associated to glaciations. In particular, deglacial meltwater induced marine stratification and enhanced nutrients supply via continental weathering, while glacial maxima would have favoured a greater flux of oxygen to the deep oceans by brine rejection and formation of cold and dense waters at high latitudes. According to their model, ocean anoxia was capable of drawing down the $CO_2$ from the ocean-atmosphere system, sustaining the early Paleozoic cold climate and preventing the onset of the greenhouse conditions that characterized most of the early Paleozoic.

Further evidence of the climatic instability associated to the Silurian time interval, in particular at the transition to the stable greenhouse conditions, is provided by the available stable oxygen isotope record described by many authors in the last decades (e.g., Bickert et al., 1997; Azmy et al., 1998; Brand et al., 2006; Lehnert et al., 2010; Trotter et al., 2016). All the available curves show large positive and negative fluctuations throughout the Rhuddanian to Homerian time interval. However, the relative influence on the observed oxygen isotope record of salinity variations, induced by global evaporation-precipitation rates and rate of continental run-off, is still a matter of debate (e.g., Bickert et al., 1997; Brand et al., 2006; Munnecke et al., 2010).

Our data, in agreement with what observed by other authors, reveal a cyclical alternation of discrete climate modes, that accompanied the transition from a cold climate to a more stable greenhouse state. The main difference between our model and the one proposed by Jeppsson (1990) is the fact that we inversely associate the humid-arid conditions on shelves with cool and warm temperatures. In fact, while Jeppsson's model supposes the presence of warm conditions during cold time intervals, we infer that warm conditions are associated with a more humid state. Even further, our model, by considering the impact of temperature on the deposition of black shales during humid conditions, is not consistent with the Bickert et al.'s (1997) model according to which temperature has limited to no effect on anoxia. On the contrary, we find many similarities with the model proposed by Page et al. (2007), where anoxia is favoured by glacio-eustatic control on water stratification and nutrient supply during warming phases occurring during deglacial transgressions.

The cycles we observed, as those distinguished by Page et al. (2007), are probably related to longer periodicities than those associated to Primo and Secundo episodes (Jeppsson, 1990; Aldridge et al., 1993; Jeppsson et al., 1995; Jeppsson, 1996, 1997) or Humid and Arid-periods (Bickert et al., 1997). However, a comparison of our results with the stratigraphic occurrences of the abovementioned episodes can be broadly correlated. During the Rhuddanian global warming, which marked the end of the Hirnantian glaciation, the major phase of glacial retreat was associated to widespread oceanic anoxia at all paleolatitudes and in a wide range of paleogeographic settings (Page et al., 2007; Le Heron et al., 2009; Melchin et al., 2013). The observed Rhuddanian-Aeronian warming trend (Interval 1), supported also by the variation in $\delta^{18}O_{phos}$ described by Trotter et al. (2016), well correspond to the interval dominated by warm Secundo episodes (i.e., Spirodden Secundo and Malmoykalven Secundo episodes) (Aldridge et al., 1993; Jeppsson, 1996). The subsequent Telychian relative cooling phase (Interval 2) is in good agreement with the Telychian glacial maximum described by Page et al. (2007) and with the shift to heavier oxygen isotope values in the Trotter et al. (2016) record. This time interval can be correlated to the cold Snipklint Primo episode (Aldridge et al., 1993; Jeppsson, 1996). The early Wenlock time interval (Interval 3) was characterized by a general warming and deposition of relatively organic-rich sediments. According to Cramer and Saltzman (2007) both the onset of the positive $\delta^{13}C$ Ireviken excursion and the beginning of a third-order transgression at the Llandovery–Wenlock transition confirm the end of the glaciation prior to the Sheinwoodian stage. The cold and arid conditions observed in our record in correspondence of the mid-upper Sheinwoodian (Interval 5), well correlate with the onset of a phase of glaciation (Lehnert et al., 2010; Loydell and Large, 2019) identifiable also on the Trotter et al. (2016) isotope record. A direct comparison for this interval with the

alternation in Primo and Secundo episodes is not easy, however a correlation with the Allekvia Primo episode (Jeppsson et al., 1995; Jeppsson, 1996) can be inferred. It must be noticed that this interval of oxic conditions was not reported by Page et al. (2007), that instead identified a persistent anoxia throughout the entire Sheinwoodian time interval. The presence of hypoxic conditions at the transition to the lowermost Homerian (Interval 6) is in agreement with Page et al. (2007). This interval can be only speculatively correlated with the warm Hellvi Secundo episode (Jeppsson et al., 1995; Jeppsson, 1996). Finally, the uppermost interval (Interval 7), characterized by stable oxic conditions, could correspond to the cooling phase recorded in the Homerian stage in correspondence of the Mulde Event (Jeppsson et al., 1995; Jeppsson, 1996; Trotter et al., 2016). The occurrence of oxic conditions that extended from the mid up to the late Homerian was reported also by Page et al. (2007).

## 6. Conclusions

The studied Silurian fine-grained record reveals the complex interaction between long-term variations in paleohydrographic settings, water column redox conditions and organic matter preservation. The deposition in a low-energy environment far from coarse sediment input allowed the preservation of a long record of bottom-water chemical variations that occurred during the climatic transition from the Ordovician cold climate to the Silurian greenhouse state. The poor connection of the epereic Baltica Sea with the Rheic Ocean favoured the onset of a limited deep-water circulation and consequent benthic anoxia. Data reveal that climatically-driven long-term variations both in pycnocline strength and nutrient supply, controlled benthic anoxia dynamics, alternating phases of deep-water hypoxia with others fully oxic. During warm-humid intervals the establishment of a stable halocline and thermocline induced the stratification of the watermass and inhibited deep-water renewal efficiency. Moreover, the increased weathering and runoff favoured the enhancement of the nutrient supply to the basin. On the contrary, during cooler and drier intervals the weakening of the pycnocline strength re-established an efficient bottom-water circulation, and the lowered weathering and runoff reduced nutrient availability. During the anoxic phases the restricted conditions favoured the formation of a deep-watermass depleted in redox-sensitive metals, thus limiting their accumulation in the sediments ("basin reservoir effect"). "Particulate-shuttle" was probably the main vector for trace-metal accumulation, as proved by the exclusive enrichment in Mo among all the redox-sensitive metals. The variation in the pycnocline strength controlled both the type of organic matter produced in the upper part of the sea as well as its faith along the water column. The presence of a stable pycnocline hampered organic matter sink, thus determining its degradation and limiting the organic carbon accumulation rate. The effect of the dynamic alternation between phases of warm and cool climatic conditions affected the redox state of the Baltica epicontinental sea over a time interval of millions of years during the transition from the Ordovician cooling to the Silurian greenhouse climate.

## Acknowledgments

We are grateful to Eni S.p.A. for permission to publish this study. We are deeply indebted with the editor Thomas Algeo and two anonymous reviewers that with their constructive comments strongly improved the quality of the manuscript.

## Data availability

Datasets related to this article can be found at https://data.mendeley.com/datasets/35rdb5j3rv/draft?a=2c941206-6808-4178-b570-2d4941ad3ec5, an open-source online data repository hosted at Mendeley Data.

## References

Aldridge, R.J., Jeppsson, L., Dorning, K.J., 1993. Early Silurian oceanic episodes and events. J. Geol. Soc. Lond. 150, 501–513.
Algeo, T.J., Heckel, P.H., 2008. The Late Pennsylvanian Midcontinent Sea of North America: a review. Palaeogeogr. Palaeoclimatol. Palaeoecol. 268, 205–221.
Algeo, T.J., Lyons, T.W., 2006. Mo–total organic carbon covariation in modern anoxic marine environments: implications for analysis of paleoredox and paleohydrographic conditions. Paleoceanography 21, PA1016. https://doi.org/10.1029/2004PA001112.
Algeo, T.J., Maynard, J.B., 2004. Trace-element behavior and redox facies in core shales of Upper Pennsylvanian Kansas-type cyclothems. Chem. Geol. 206, 289–318.
Algeo, T.J., Rowe, H., 2012. Paleoceanographic applications of trace-metal concentration data. Chem. Geol. 324–325, 6–18.
Algeo, T.J., Tribovillard, N., 2009. Environmental analysis of paleoceanographic systems based on molybdenum–uranium covariation. Chem. Geol. 268, 211–225.
Algeo, T.J., Heckel, P.H., Maynard, J.B., Blakey, R., Rowe, H., 2008. Modern and ancient Epicratonic Seas and the superestuarine circulation model of marine anoxia. In: Holmden, C., Pratt, B.R. (Eds.), Dynamics of Epeiric Seas: Sedimentological, Paleontological and Geochemical Perspectives. Geological Association of Canada Special Publication, vol. 48. pp. 7–38.
Azmy, K., Veizer, J., Bassett, M.G., Popper, P., 1998. Oxygen and carbon isotopic composition of Silurian brachiopods: implications for coeval seawater and glaciations. GSA Bull. 110, 1499–1512.
Bickert, T., Pätzold, J., Samtleben, C., Munnecke, A., 1997. Paleoenvironmental changes in the Silurian indicated by stable isotopes in brachiopod shells from Gotland, Sweden. Geochim. Cosmochim. Acta 61, 2717–2730. https://doi.org/10.1016/S0016-7037(97)00136-1.
Brand, U., Azmy, K., Veizer, J., 2006. Evaluation of the Salinic I tectonic, Cancaniri glacial and Ireviken biotic events: Biochemostratigraphy of the Lower Silurian succession in the Niagara Gorge area, Canada and U.S.A. Palaeogeogr. Palaeoclimatol. Palaeoecol. 241, 192–213.
Bromley, R.G., Ekdale, A.A., 1984. Chondrites: a trace fossil indicator of anoxia in sediments. Science 224, 872–874.
Calner, M., 2008. Silurian global events - at the tipping point of climate change. In: Ashraf, M.T. Elewa (Ed.), Mass extinctions. Springer-Verlag, Berlin and Heidelberg, pp. 21–58.
Cramer, B.D., Saltzman, M.R., 2005. Sequestration of $^{12}C$ in the deep ocean during the early Wenlock (Silurian) positive carbon isotope excursion. Palaeogeogr. Palaeoclimatol. Palaeoecol. 219, 333–349.
Cramer, B.D., Saltzman, M.R., 2007. Fluctuations in epeiric sea carbonate production during Silurian positive carbon isotope excursions: a review of proposed paleoceanographic models. Palaeogeogr. Palaeoclimatol. Palaeoecol. 245, 37–45.
Delabroye, A., Vecoli, M., Hints, H., Servais, T., 2011. Acritarchs from the Ordovician-Silurian Boundary Beds of the Valga-10 Drill Core, Southern Estonia (Baltica) and their Stratigraphical and Palaeobiogeographical implications. Palynology 35 (1), 4–45.
Egenhoff, S., Maletz, J., 2007. Graptolites as indicators of maximum flooding surfaces in monotonous deep-water shelf sequences. PALAIOS 22, 373–383.
Fagel, N., 2007. Marine clay minerals, deep circulation and climate. In: Hilaire-Marcel, C., De Vernal, A. (Eds.), Paleoceanography of the Late Cenozoic. Methods 1. Elsevier, Amsterdam, pp. 25.
Gambacorta, G., Menichetti, E., Trincianti, E., Torricelli, S., 2018. Orbital control on cyclical primary productivity and benthic anoxia: astronomical tuning of the Telychian Stage (early Silurian). Palaeogeogr. Palaeoclimatol. Palaeoecol. 495, 152–162.
Ganeshram, R.S., Calvert, S.E., Pedersen, T.F., Cowie, G.L., 1999. Factors controlling the burial of organic carbon in laminated and bioturbated sediments off NW Mexico: implications for hydrocarbon preservation. Geochim. Cosmochim. Acta 63, 1723–1734.
Goldman, D., Maletz, J., Melchin, M.J., Junxuan, F., 2013. Graptolite palaeogeography. In: Harper, D.A.T., Servais, T. (Eds.), Early Palaeozoic Biogeography and Palaeogeography. Geological Society, London, Memoirs, vol. 38. pp. 415–428.
Jachowicz, M., 2000. Acritarch assemblages from the Silurian Pomeranian Caledonides and their foreland. Geol. Q. 44, 317–331.
Jaworowski, K., 2000. Facies analysis of the Silurian shale-siltstone succession in Pomerania (northern Poland). Geol. Q. 44, 297–315.
Jeppsson, L., 1990. An oceanic model for lithological and faunal changes tested on the Silurian record. J. Geol. Soc. 147, 663–674.
Jeppsson, L., 1996. Recognition of a probable secundo-primo event in the early Silurian. Lethaia 29, 311–315.
Jeppsson, L., 1997. The anatomy of the Mid–early Silurian Ireviken Event and a scenario for P–S events. In: Brett, C.E., Baird, G.C. (Eds.), Paleontological Events: Stratigraphic, Ecological, and Evolutionary Implications. Columbia University Press, New York, pp. 451–492.
Jeppsson, L., Aldridge, R.J., Dorning, K.J., 1995. Wenlock (Silurian) oceanic episodes and events. J. Geol. Soc. Lond. 152, 487–498.
Jones, B., Manning, D.A.C., 1994. Comparison of geochemical indices used for the interpretation of palaeoredox conditions in ancient mudstones. Chem. Geol. 111, 111–129.
Kellerhals, T., Tobler, L., Brütsch, S., Sigl, M., Wacker, L., Gäggeler, H.W., Schwikowski, M., 2010. Thallium as a tracer for preindustrial volcanic eruptions in an ice core record from Illimani, Bolivia. Environ. Sci. Technol. 44, 888–893.
Koinig, K.A., Shotyk, W., Lotter, A.F., Ohlendorf, C., Sturm, M., 2003. 9000 years of geochemical evolution of lithogenic major and trace elements in the sediment of an

alpine lake–the role of climate, vegetation, and land-use history. J. Paleolimnol. 30, 307–320.
Le Hérissé, A., 1989. Acritarches et kystes d'algues Prasinophycées du Silurien de Gotland, Suède. Palaeontographia Italica 76, 57–302.
Le Heron, D.P., Craig, J., Etienne, J.L., 2009. Ancient glaciations and hydrocarbon accumulations in North Africa and the Middle East. Earth-Sci. Rev. 93, 47–76.
Lehnert, O., Männik, P., Joachimski, M.M., Calner, M., Frýda, J., 2010. Palaeoclimate perturbations before the Sheinwoodian glaciation: a trigger for extinctions during the 'Ireviken Event'. Palaeogeogr. Palaeoclimatol. Palaeoecol. 296, 320–331.
Liu, Z., Algeo, T.J., Guo, X., Fan, J., Du, X., Lu, Y., 2017. Paleo-environmental cyclicity in the early Silurian Yangtze Sea (South China): tectonic or glacio-eustatic control? Palaeogeogr. Palaeoclimatol. Palaeoecol. 466, 59–76.
Loydell, D.K., Large, R.R., 2019. Biotic, geochemical and environmental changes through the early Sheinwoodian (Wenlock, Silurian) carbon isotope excursion (ESCIE), Buttington Quarry, Wales. Palaeogeogr. Palaeoclimatol. Palaeoecol. 514, 305–325.
Masiak, M., Podhalańska, T., Stempień-Sałek, M., 2003. Ordovician-Silurian Boundary in the Bardo Syncline, Holy Cross Mountains, Poland – new data on fossil assemblages and sedimentary succession. Geol. Q. 47, 311–331.
McArthur, A.D., Kneller, B.C., Souza, P.A., Kuchle, J., 2016. Characterization of deep-marine channel-leeve complex architecture with palynofacies: an outcrop example from the Rosario Formation, Baja California, Mexico. Mar. Pet. Geol. 73, 157–173.
Melchin, M.J., Mitchell, C.E., Holmden, C., Štorch, P., 2013. Environmental changes in the late Ordovician–early Silurian: review and new insights from black shales and nitrogen isotopes. GSA Bull. 125, 1635–1670.
Moczydłowska, M., 2008. New records of late Ediacaran microbiota from Poland. Precambrian Res. 167, 71–92.
Modliński, Z., Podhalańska, T., 2010. Outline of the lithology and depositional features of the lower Paleozoic strata in the polish part of the Baltic region. Geol. Q. 54, 109–121.
Modliński, Z., Szymański, B., Teller, L., 2006. Silurian lithostratigraphy in the polish part of the Peribaltic Depression – continental and marine parts (N Poland). Prz. Geol. 54, 787–796.
Molyneux, S., Barron, H., Smith, R., 2008. Upper Llandovery-Wenlock (Silurian) palynology of the Pentland Hills inliers, Midland Valley of Scotland. Scott. J. Geol. 44, 151–168.
Munnecke, A., Calner, M., Harper, D.A.T., Servais, T., 2010. Ordovician and Silurian Seawater chemistry, sea level, and climate: a synopsis. Palaeogeogr. Palaeoclimatol. Palaeoecol. 296, 389–413.
Okrugin, V., Favero, M., Liu, A., Etschmann, B., Plutachina, E., Mills, S., Tomkins, A.G., Lukasheva, M., Kozlov, V., Moskaleva, S., Chubarov, M., Brugger, J., 2017. Smoking gun for thallium geochemistry in volcanic arcs: Nataliyamalikite, TlI, a new thallium mineral from an active fumarole at Avacha Volcano, Kamchatka Peninsula, Russia. Am. Mineral. 102, 1736–1746.
Oppenheimer, C., 2011. Eruptions that Shook the World. Cambridge University Press, Cambridge (UK) (406 pp.).
Page, A.A., Zalasiewicz, J.A., Williams, M., Popov, L.E., 2007. Were transgressive black shales a negative feedback modulating glacioeustasy in the early Paleozoic icehouse? In: Williams, M., Haywood, A.M., Gregory, F.J., Schmidt, D.N. (Eds.), Deep-time Perspectives on Climate Change: Marrying the Signal From Computer Models and Biological Proxies. The Micropalaeontological Society, Special Publications Geological Society, London, pp. 123–156.
Piper, D.Z., Calvert, S.E., 2009. A marine biogeochemical perspective on black shale deposition. Earth Sci. Rev. 95, 63–96.
Pohl, A., Donnadieu, Y., Le Hir, G., Ferreira, D., 2017. The climatic significance of late Ordovician–early Silurian black shales. Paleoceanography Paleoclimatology. https://doi.org/10.1002/2016PA003064.
Porębski, S.J., Prugar, W., Zacharski, J., 2013. Silurian shales of the east European Platform in Poland – some exploration problems. Prz. Geol. 61 (11/1), 630–638.
Prauss, M., Riegel, W., 1989. Evidence from phytoplankton associations for causes of black shale formation i epicontinental seas. Neues Jb. Geol. Paläontol. Monat. 11, 671–682.
Rowe, H.D., Loucks, R.G., Ruppel, S.C., Rimmer, S.M., 2008. Mississippian Barnett Formation, FortWorth Basin, Texas: bulk geochemical inferences and Mo–TOC constraints on the severity of hydrographic restriction. Chem. Geol. 257, 16–25.
Sageman, B.B., Lyons, T.W., 2005. Geochemistry of Fine-grained Sediments and Sedimentary Rocks. In: Holland, H.D., Turekian, K.K. (Eds.), Sediments, Diagenesis, and Sedimentary Rocks. Treatise on Geochemistry, vol. 7. Elsevier, Amsterdam, pp. 115–158.
Schneider, R.R., Price, B., Müller, P.J., Kroon, D., Alexander, I., 1997. Monsoon related variations in Zaire (Congo) sediment load and influence of fluvial silicate supply to productivity in the east equatorial Atlantic during the last 200,000 years. Paleoceanography 12, 463–481.
Seilacher, A., 1967. Bathymetry of trace fossils. Mar. Geol. 5, 413–428.
Sweere, T., van den Boorn, S., Dickson, A.J., Reichart, G.-J., 2016. Definition of new trace-metal proxies for the controls on organic matter enrichment in marine sediments based on Mn, Co, Mo and Cd concentrations. Chem. Geol. 441, 235–245.
Thyberg, B.I., Jordt, H., Bjørlykke, K., Faleide, J.I., 2000. Relationships between sequence stratigraphy, mineralogy and geochemistry in Cenozoic sediments of the northern North Sea. Geol. Soc. Lond. Spec. Publ. 167, 245–272.
Torsvik, T.H., Cocks, L.R.M., 2016. Earth History and Palaeogeography. Cambridge University Press, Cambridge, United Kingdom (332 pp.).
Trela, W., Bąk, E., Pańczyk, M., 2017. Upper Ordovician and Silurian ash beds in the Holy Cross Mountains, Poland: preservation in mudrock facies and relation to atmospheric circulation in the Southern Hemisphere. J. Geol. Soc. https://doi.org/10.1144/jgs2017-026.
Tribovillard, N., Algeo, T.J., Lyons, T., Riboulleau, A., 2006. Trace metals as paleoredox and paleoproductivity proxies: an update. Chem. Geol. 232, 12–32.
Tribovillard, N., Bout-Rouzmazeilles, V., Algeo, T., Lyons, T.W., Sionneau, T., Montero-Serrano, J.C., Riboulleau, A., Baudin, F., 2008. Paleodepositional conditions in the Orca Basin as inferred from organic matter and trace metal content. Mar. Geol. 254, 62–72.
Tribovillard, N., Algeo, T.J., Baudin, F., Riboulleau, A., 2012. Analysis of marine environmental conditions based on molybdenum-uranium covariation – applications to Mesozoic paleoceanography. Chem. Geol. 324–325, 46–58.
Trotter, J.A., Williams, I.S., Barnes, C.R., Männik, P., Simpson, A., 2016. New conodont $\delta^{18}O$ records of Silurian climate change: implications for environmental and biological events. Palaeogeogr. Palaeoclimatol. Palaeoecol. 443, 34–48. https://doi.org/10.1016/j.palaeo.2015.11.011.
Tyson, R.V., 1995. Sedimentary Organic Matter. Organic Facies and Palynofacies. Chapman & Hall, London (615 pp.).
Vecoli, M., Riboulleau, A., Versteegh, G.J.M., 2009. Palynology, organic geochemistry and carbon isotope analysis of a latest Ordovician through Silurian clastic succession from borehole Tt1, Ghadamis Basin, southern Tunisia, North Africa: palaeoenvironmental interpretation. Palaeogeogr. Palaeoclimatol. Palaeoecol. 273, 378–394.
Warny, S., Wrenn, J.H., Bart, P.J., Askin, R., 2006. Palynology of the NBP03-01A transect in the Northern Basin, Western Ross Sea, Antarctica: a late Pliocene record. Palynology 30, 1–32.
Wedepohl, K.H., 1971. Environmental influences on the chemical composition of shales and clays. In: Ahrens, L.H., Press, F., Runcorn, S.K., Urey, H.C. (Eds.), Physics and Chemistry of the Earth, vol. 8. Pergamon, Oxford, pp. 305–333.
Wedepohl, K.H., 1991. The composition of the upper earth's crust and the natural cycles of selected metals. Metals in natural raw materials. Natural resources. In: Merian, E. (Ed.), Metals and their Compounds in the Environment. VCH, Weinheim, pp. 3–17.
Whitaker, M.F., Giles, M.R., Cannon, S.J.C., Morton, A.C., 1992. Palynological review of the Brent Group, UK sector, North Sea. In: Haszeldine, R.S., Giles, M.R., Brown, S. (Eds.), Geology of the Brent Group. Geological Society Special Publication, vol. 61. pp. 169–202.
Wicander, R., Wood, G.D., 1997. The use of microphytoplankton and chitinozoans for interpreting transgressive/regressive cycles in the Rapid Member of the Cedar Valley Formation (Middle Devonian), Iowa. Rev. Palaeobot. Palynol. 98, 125–152.